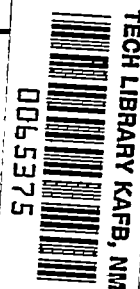


3552

NACA TN 2126



# NATIONAL ADVISORY COMMITTEE FOR AERONAUTICS

TECHNICAL NOTE 2126

IMPROVEMENTS IN HEAT TRANSFER FOR ANTI-ICING OF GAS-HEATED  
AIRFOILS WITH INTERNAL FINS AND PARTITIONS

By Vernon H. Gray

Lewis Flight Propulsion Laboratory  
Cleveland, Ohio



Washington

July 1950

AFMTC  
TEST LIBRARY  
44-4503

319.98/41



## TECHNICAL NOTE 2126

IMPROVEMENTS IN HEAT TRANSFER FOR ANTI-ICING OF GAS-HEATED  
AIRFOILS WITH INTERNAL FINS AND PARTITIONS

By Vernon H. Gray

## SUMMARY

The effect of modifying the gas passage of hollow metal airfoils by the addition of internal fins and partitions was experimentally investigated and comparisons were made among a basic unfinned airfoil section and two airfoil designs having metal fins attached at the leading edge of the internal gas passage. An analysis considering the effects of heat conduction in the airfoil metal was made to determine the internal modification effectiveness that may be obtained in gas-heated components, such as turbojet-inlet guide vanes, support struts, hollow propeller blades, and thin wings.

Over a wide range of heated-gas flow and tunnel-air velocity, the increase in surface-heating rates with internal finning was marked (up to 3.5 times), with the greatest increase occurring at the leading edge where anti-icing heat requirements are most critical. Variations in the amount and the location of internal finning and partitioning provided control over the local rates of surface heat transfer and permitted efficient anti-icing utilization of the gas-stream heat content.

## INTRODUCTION

Surface-ice prevention by the use of hot gas flowing through hollow airfoil shapes has long been considered because of advantages in weight, simplicity, availability of heating medium, and durability of installation. Use of the hot-gas method of anti-icing has been restricted, however, partly because of difficulty in controlling the rate of heat dissipation over the chordal and spanwise extent of the airfoil. A facility for concentrating the flow of heat toward the leading-edge surfaces, where the heat requirement for anti-icing is greatest, has been lacking. This deficiency has been analytically and experimentally observed and is reported in references 1 to 5.

An investigation was conducted at the NACA Lewis laboratory to evaluate by experimental comparisons the effect of internal fins and partitions on the anti-icing qualities of gas-heated airfoil sections, applicable to such components as turbojet-inlet guide vanes, support struts, propeller blades, and thin wings. Heat-transfer investigations were made in a two-dimensional duct tunnel on two designs of finned airfoil sections as compared with an unfinned section. Increases in airfoil surface temperatures above tunnel-air temperatures were measured for various rates of gas heating, for immersion in both dry and wet air streams, and at airspeeds up to 300 miles per hour. Because of simpler and more accurate experimental procedures, most of the data presented are for dry air. The results obtained for dry air were applied to anti-icing performance by use of the wet-air analysis given in reference 1. The three airfoil sections were analyzed to evaluate the important effects of heat conduction in the metal and the variations of convective heat-transfer rates in spanwise and chordwise directions. Surface-heating improvement factors are presented for two modified airfoil sections as compared with the original airfoil section.

## APPARATUS AND AIRFOILS

### Installation

The duct tunnel used for the gas-heating investigations is shown in figure 1. Atmospheric air was induced through the tunnel by suction from a centrifugal blower. The transparent test section measured 2 by 20 inches.

The airfoil sections were mounted in the center of the test section, as shown in figure 2. The hot-gas supply for the models was ducted through a rectangular diffuser, the approach section, the model airfoil section, and the exit section. Contours of the approach section, the exit section, and the openings in the insulated side plates approximately matched the internal passage through the unfinned airfoil section. Small differences in the contours and slight misalignment of the assembly resulted, however, with attendant disturbances to the internal-flow boundary-layer characteristics. The hot gas was supplied from a compressed-air system and was piped through a calibrated orifice, a regulating valve, an electric heater, and then through a duct to the diffuser and the models.

Above-freezing cloud conditions were simulated in the tunnel by the use of a water-spray nozzle located at the tunnel inlet. Calibrations of the nozzle indicated that average cloud conditions at the tunnel center line just ahead of the models were approximately as follows: volume-median droplet diameter, 15 to 20 microns; liquid-water content at 275 miles per hour, 1.3 grams per cubic meter; liquid-water content at 100 miles per hour, 1.7 grams per cubic meter.

### Airfoil sections

Details and dimensions of the three airfoil sections investigated are presented in figure 3 and table I. An NACA 0012 symmetrical airfoil section was selected for investigation because it is a basic shape about which other icing information is known and may be considered somewhat representative of propeller-blade sections, struts, wings, and the fore part of turning vanes.

Airfoil section A is a hollow steel section with an insulating partition starting at 0.46 chord. Section B is the same as section A, with the addition of two sheet-metal fins that are attached to the leading edge. Section C has shorter and thicker fins that are tapered toward the tips and an enlarged center partition to reduce the gas-flow-passage area. When the airfoil is assembled with the tunnel side walls, the hollow region behind the partition becomes a dead-air chamber.

### Instrumentation

Surface-temperature thermocouples were installed on the sections in 16 locations (fig. 3). One metal temperature thermocouple was located at the leading edge of the internal passage of each section and one thermocouple was installed at the tip of one fin of both finned sections. The tunnel-air temperature was measured at the tunnel inlet and two fixed gas-temperature rakes of four bare thermocouples each were located on the gas-passage center line (fig. 2).

Iron-constantan thermocouple junctions were spot-welded to the airfoil metal surfaces. The leads were rolled to a thickness of approximately 0.003 inch and attached to and insulated from the metal by a thin coating of cement. From the junctions, the leads extended to corresponding holes in the side wall (fig. 2).

The total protrusion of thermocouples and leads above the metal surface was approximately 0.007 inch. The installations were faired into the airfoil contour as much as possible and an effort was made to keep the metal surfaces clean.

Inasmuch as all the models were symmetrical and at zero angle of attack, the upper and lower surface thermocouples yielded very nearly the same temperature patterns and served as a check on the instrumentation.

#### PRELIMINARY CONSIDERATIONS

##### Thermocouple Attachment and Surface Coating

Gas-heated airfoils are difficult to provide with accurate surface-temperature instrumentation. If the thermocouple junction and adjacent leads protrude into either the air or hot-gas stream, an appreciable error may be introduced by heat conduction along the leads. Projecting leads can also seriously disturb the stream-flow characteristics, such as causing transition to turbulent flow in the air stream and blockage to the gas-stream flow. Even if the thermocouple leads were fully embedded beneath the surface, their tunnels in the thin metal skin would still constitute heat barriers disruptive to the normal skin-temperature gradients. By simpler means, the instrumentation may be completely covered with a smooth surface coating, such as paint, that will minimize most of the aforementioned difficulties. Unfortunately, the temperature gradient through the surface coating is introduced as a new problem. Such a coating removes the thermocouple from the exposed surface and leaves doubt as to the actual surface temperature.

In order to obtain a measure of these surface-temperature errors, a preliminary comparison was made under the same flow and heating conditions between section A with bare instrumentation, as previously described, and with the same instrumented section externally coated with aircraft primer and a final coat of black lacquer so that no surface irregularities remained. The paint thickness was approximately 0.010 inch, which was sufficient to cover the thermocouples by about 0.003 inch. This paint coating is similar in application to that of many propellers and wings in use and has also been used in previous icing investigations.

The effect of the paint coating is illustrated in figure 4; where the chordwise variation of surface-temperature rise above dry tunnel-air temperature is plotted for the bare and painted section A at two flow conditions. The painted airfoil indicated the higher surface temperatures; the greatest increase over the bare model occurred at the leading edge and at the highest values of gas flow and air velocity investigated. The greatest and smallest differences in stagnation-point temperatures between the two models were determined from data not shown as approximately  $50^{\circ}$  and  $30^{\circ}$  F, respectively. During icing conditions, however, calculations indicate that these differentials would be reduced to the order of  $15^{\circ}$  to  $10^{\circ}$  F.

Because the maximum paint effect occurred at the leading edge, the gradient through the paint coating and the reduced conductive loss in the thermocouple leads were believed to account for most of the paint effect and the improved surface smoothness was of lesser importance. Thermal-conductivity values for paints are too uncertain to allow calculation of temperature gradients through paint films for known rates of heat transfer. The available information, however, indicates that more than half of the observed temperature increase with surface painting is due to the thermal gradient in the paint film and that the balance is caused by local thermocouple errors inherent in the bare surface-thermocouple installation.

These comparisons illustrate that thermocouples attached to a metal surface and covered with a faired coating of paint or cement will indicate temperatures several degrees higher than the exposed surface, which, for example, may be undergoing icing while safe anti-icing temperatures are being indicated. Thus, to insure conservative surface-temperature indication, the bare surface-thermocouple installation was employed in this investigation, with care taken that the leads were rolled as fine (0.003 in. thick) as durability considerations permitted.

#### Datum Air Temperature

The local kinetic, or datum air, temperature  $t_a$  over the models in the dry-air investigations was taken as the constant value indicated by the static-air-temperature thermocouple at the tunnel inlet. (All symbols used throughout this report are defined in the appendix.) This simplification avoids calculation of adiabatic temperature drops, local velocities, and kinetic-recovery coefficients. For the range of airspeeds involved, this

approximation may entail a maximum theoretical error of 3° F. For an experimental check on the kinetic heating effect, the models were subjected to the maximum air velocity  $V_0$  of 300 miles per hour with zero gas flow. The surface thermocouples indicated temperatures within 1° F and the tunnel-inlet thermocouple indicated a maximum disagreement of  $1\frac{1}{2}$ ° F with the average model-surface temperature. By considering the magnitude of the surface-temperature-rise differentials that usually resulted in the investigations, this approximation of air temperature was deemed satisfactory for all cases.

The preceding discussion applies equally well to the effective gas temperatures, as indicated by the gas-temperature probes, because of the relatively low maximum gas velocity (110 mph) and negligible amounts of radiation at the operating temperatures.

In the few wet-air investigations, the datum air temperature  $t_a$  in the spray cloud was determined from a calibration of unheated model temperatures taken over a range of air velocities, liquid-water contents, and dry-air temperatures at the tunnel inlet. No measurements of the tunnel-air humidity were made during the calibration; consequently, the datum temperatures in the wet-air investigations were less reliable than in the dry-air cases.

The trailing-edge surface temperatures have not been plotted in the subsequent figures. The trailing half of each section exhibited a rapidly decreasing surface temperature, which at the trailing edge approached the datum air temperature to within a maximum difference of 35° F (section C, gas flow of 325 lb/hr and air velocity of 102 mph).

#### Conduction Losses

Because of the narrowness of the duct tunnel, thermal conduction from the heated region of the models to the insulated side supports and the trailing half of the models was suspected of influencing the temperature indication at the model center lines. A "no-load" investigation indicated that the losses due to conduction into the side walls appreciably affected the surface-temperature indication. A thorough calibration was not made, however, and the indicated values of surface temperature are presented in the subsequent analysis. The error involved is greatest at the low air velocities and regions near the midpoint of chord; neither case is critical to anti-icing performance.

## CONDITIONS AND PROCEDURE

The airfoil-surface-temperature patterns over each of the three models were obtained in dry tunnel air at velocities  $V_0$  of 102, 160, 210, and 275 miles per hour, gas-flow rates  $w$  of 100 and 325 pounds per hour, and a mean gas temperature  $t_{g,m}$  of 370° F. Surface temperatures were also taken in dry air at a velocity of 300 miles per hour with gas flows of 100, 150, 240, and 325 pounds per hour through each of the sections and with the same mean gas temperature. In order to determine the effect of gas temperature, surface temperatures of each section were obtained in dry air at a velocity of 102 miles per hour for a range of mean gas temperatures from 125° to 375° F. The datum air temperature ranged between 32° and 80° F.

For the aforementioned conditions and throughout the heat-transfer analysis and discussion, dry tunnel-air conditions are presented. Only a few comparisons are made with wet-air conditions in the tunnel to afford a check on the analysis of anti-icing heat requirements. Wet-surface temperatures over the three airfoil sections were taken at tunnel-air velocities of 102 and 275 miles per hour with gas flows of both 100 and 325 pounds per hour. Wet datum air temperatures were obtained between 35° and 63° F.

Steady-state flow was established for each condition by allowing at least 10 minutes between any significant change in flow or temperature values and the recording of data. Consistency of the data was good, with reruns of the same conditions agreeing within an average discrepancy in surface temperature of 3° F. The recording potentiometer was considered accurate to within  $\pm 2^\circ$  F.

## ANALYSIS OF RESULTS

## Typical Results

The rise in surface temperature above the datum air temperature for the three airfoil sections at various flow conditions is shown in figure 5. Comparisons may be made directly among the following conditions: (a) airfoil sections A, B, and C with the same heating and flow conditions in which the increased surface heating due to internal fins and partitions is clearly evident; (b) section C with air velocities of 275 and 102 miles per hour but with the same gas-flow rate and temperature, illustrating the magnitude of air-velocity effect; (c) section B with gas flows of 325 and 100 pounds per hour and the same air velocity and gas

temperature; and (d) section C with dry and wet tunnel air and the same heating and flow rates. Comparison (d) shows that the airfoil leading edge in cloud conditions was considerably chilled by evaporation of impinging moisture but the surface became effectively dry at approximately 3.5 inches from stagnation and the two surface-temperature curves very nearly coincided beyond that point.

The surface-temperature rise at the stagnation point of the three airfoil sections as a function of the gas-temperature differential  $t_{g,m}-t_a$  is shown in figure 6. Data are presented for section C in both dry- and wet-air conditions. This figure confirms the expected linear relation between gas temperature and surface temperature, other conditions being constant, and indicates the consistency and reliability of the installation and the instrumentation used. The three dry-air examples show data points scattered less than  $\pm 5$  percent from the plotted straight lines. The wet-air curve indicates the progressive reduction in surface-temperature rise for increments of increasing gas-temperature differential, caused by the dependence of surface-evaporation rate on actual surface temperatures.

#### Effectiveness of Internal Fins and Partitions

The effectiveness of gas-heated airfoils with internal-fin modifications in anti-icing can be measured by comparing, under the same conditions, a finned section with an unfinned section in regard to (a) increased surface heating rates and (b) reduced heated-gas requirements. With fins, the increase of the surface heat-transfer rate for a fixed condition of air and gas flows can be determined from the surface-temperature rise above the datum air temperature  $t_s-t_a$  because in dry air the heat-transfer coefficient is nearly constant over the normal range of temperatures. Thus,

$$q_a = h_a(t_s-t_a) \approx C_1(t_s-t_a) \quad (1)$$

Similarly, with fins, the decrease in the required heat content of the internal gas flow for a fixed condition of blade-surface heat transfer can be determined from the gas-flow rate if the mean gas temperature is held constant, or

$$Q_I = wc_p(t_{g,m}-t_a) = C_2w \quad (2)$$

Modification effectiveness. - If equation (1) is considered, a comparison of surface heat transfer between finned and unfinned airfoil sections can be expressed by the ratio

$$\frac{q_{a,f}}{q_{a,u}} = e \approx \frac{(t_s - t_a)_f}{(t_s - t_a)_u} \quad (3)$$

that may be termed modification effectiveness. The chordwise variation of local modification effectiveness, as indicated for the finned sections B and C, is plotted in figure 7 for various flow conditions. The increased heat transfer through finned sections was marked. In each case, the improvement was greatest in the region of the stagnation point, the area most critical for anti-icing of gas-heated airfoils. The increase in surface heat transfer, denoted by  $e$ , reached a maximum of 3.5 at the leading edge of section C. The increase at the stagnation point was from 30 to 80 percent greater than for the average of the whole heated-surface area. The fin design of section C was always more effective in increasing surface heat transfer than was section B.

Inspection of the variables involved in figure 7 shows that modification effectiveness increased with air velocity, decreased with increasing gas flow, and was substantially independent of the gas-temperature differential  $t_{g,m} - t_a$ . Accordingly, the modification effectiveness was investigated as a function of the external to internal flow ratio  $v/w$  and correlated well when plotted as a function of the nondimensional mass-velocity ratio  $g_0 v_0 / G_u = Y$  (fig. 8). The improvement in surface heat transfer due to the addition of the internal configurations investigated for sections B and C is also shown in figure 8.

Relative modification effectiveness. - Another concept of modification effectiveness, a comparison of the internal effective conductance  $h_g A_g$  between modified and unmodified airfoil sections, may also be applied. The effective conductance of heat from the gas stream to internally convoluted airfoil sections cannot be easily determined by theoretical means but can be experimentally determined by its external effects. For simplicity, a negligible temperature gradient is assumed in the heat-flow path across the airfoil skin material in the following equations; in some cases, however, the gradient has an appreciable effect as will be subsequently shown:

$$Q_g = h_g A_g (t_{g,m} - t_s)_{av} \quad (4)$$

Also,

$$Q_a = h_{a,av} A_a (t_s - t_a)_{av} \quad (5)$$

Assuming no spanwise conduction and no chordwise conduction except within the heated area gives

$$Q_g = Q_a \quad (6)$$

and

$$h_g A_g = h_{a,av} A_a \frac{(t_s - t_a)_{av}}{(t_{g,m} - t_s)_{av}} \quad (7)$$

or

$$\frac{(h_g A_g)_f}{(h_g A_g)_u} = \frac{(h_{a,av} A_a)_f (t_s - t_a)_{av,f} (t_{g,m} - t_s)_{av,u}}{(h_{a,av} A_a)_u (t_s - t_a)_{av,u} (t_{g,m} - t_s)_{av,f}} \quad (8)$$

Furthermore, the following equation is given in reference 6 for fully developed turbulent flow in long tubes:

$$h_g = 4.1 \times 10^{-4} \frac{T_{g,m}^{0.3} v_w^{0.8} p^{0.2}}{A_p} \quad (9)$$

From reference 7, for laminar air flow over plates,

$$h_a = 0.0562 \sqrt{\frac{T_s + T_a}{2}} \sqrt{\frac{v_{av} \rho_0 g}{S}} \quad (10)$$

for air flow normal to the leading-edge cylinder,

$$h_a = 0.194 \left( \frac{T_s + T_a}{2} \right)^{0.49} \left( \frac{v_0 \rho_0 g}{D_c} \right)^{0.50} \left( 1 - \left| \frac{\Phi}{90} \right|^3 \right) \quad (11)$$

and for turbulent flow over plates,

$$h_a = 0.524 \left( \frac{T_s + T_a}{2} \right)^{0.3} \left( \frac{v_{av}^{0.08}}{S^{0.25}} \right)^{0.8} \quad (12)$$

From equations (8) and (10) to (12), the external effective conductance  $h_{a,av}A_a$  is seen to be essentially constant between finned and unfinned airfoil sections compared at the same flow conditions. The slight dependence of  $h_a$  on  $t_s$  is unimportant and is neglected in these calculations. Accordingly, equation (8) reduces to

$$\frac{(h_g A_g)_f}{(h_g A_g)_u} = E \approx \frac{(t_s - t_a)_{av,f} (t_{g,m} - t_s)_{av,u}}{(t_s - t_a)_{av,u} (t_{g,m} - t_s)_{av,f}} \quad (13)$$

The factor  $E$  in equation (13) can thus be determined as the surface-average modification effectiveness  $e_{av}$  multiplied by the unfinned-to-finned-section ratio of the gas-to-surface temperature differential  $(t_{g,m} - t_s)_{av}$ . With the factor  $E$ , data taken at different values of gas temperature can be related on a common basis. The data in figure 8 are replotted in terms of the factor  $E$  in figure 9. The values of  $E$  at the stagnation point were calculated using equations (4) to (6) and (13) for point values as was done for integrated averages over the heated-surface area.

The curves for the heated-surface averages in figure 9 approach constancy with the mass-velocity ratio  $Y$ . The variation of  $E$  with  $Y$  is due to the temperature gradient through the metal skin, which was neglected in the derivation of  $E$ . The greatest variation is in the curves for the stagnation-point values, resulting from the large leading-edge temperature gradients.

Representative values of the factor  $E$ , based on typical operating flow conditions, may be taken as constants over the flow ranges to be expected. These values are presented in the following table:

Airfoil section	Relative modification effectiveness	
	E	
	Heated-surface average	Stagnation point
B	1.6	2.4
C	2.6	3.7

Gas-flow reduction with internal modifications. - Another method of comparing the effectiveness of finned and unfinned airfoil sections is by the rate of heated-gas flow required. As shown in equation (2), the gas-flow rate  $w$  is a measure of the heat content of the gas flow based on a constant gas-temperature differential  $t_{g,m} - t_a$ . In figure 10, the average values of heated-surface temperature rises  $(t_s - t_a)_{av}$  for the three airfoil sections at various rates of gas flow  $w$  are shown. These surface-temperature values are for a constant air velocity of 300 miles per hour and give a measure of the external-surface total heat transfer, as can be seen from equations (1) and (5). A comparison can therefore be made by determining the gas flow through a finned section  $w_f$  that will produce the same average surface-temperature rise  $(t_s - t_a)_{av,f}$  as results from a given gas flow through an unfinned section  $w_u$ . The ratio of these two flow rates  $R = w_f/w_u$  will thus express the reduction in gas heating required for a given airfoil-surface total heat transfer when internal fins and partitions are added to an airfoil section. This gas-flow ratio  $R$  was found from the data of figure 10 to be nearly independent of the absolute value of gas-flow rates. Representative values of the ratio  $R$ , indicative of the flow conditions investigated, may be selected as 0.36 and 0.14 for sections B and C, respectively.

As discussed in reference 1, the gas-flow ratio  $R$  can be theoretically approximated by the equation

$$\frac{w_f}{w_u} \approx \left( \frac{A_{g,u}}{A_{g,f}} \right)^{1.5} \left( \frac{A_{p,f}}{A_{p,u}} \right)^{1.25} \quad (14)$$

By substituting values from table I, the flow ratio from equation (14) becomes 0.28 for section B and 0.18 for section C. The representative experimental value of  $R$  satisfactorily agrees with the theoretical value for section C but disagrees for section B

because the relatively thin and long fins of this section operate inefficiently. In deriving equation (14), the assumption is made that the airfoil internal heat-transfer area  $A_g$  is determined by the gas-passage perimeter  $P$  measured around the fins. Unless the fins are very effective, the term  $A_{g,f}$  becomes too large and results in flow-ratio values that are too small. According to reference 8, the fin length  $L_f$  (measured from root to tip) becomes unimportant in uniform-thickness fins for values of the term  $2h_g L_f^2 / kd$  larger than 4.0. The lowest value of this term applicable to section B is approximately 12; therefore, equation (14) does not apply to section B.

An unfinned-airfoil segment required to deliver heat to the external surface at a rate sufficient for anti-icing could have its internal gas flow reduced by approximately 64 and 86 percent, respectively, when internally modified similar to sections B and C and when the total heat transfer throughout the heated-surface area is constant. The corresponding increases in gas-temperature drop through the segments would be the reciprocal of  $R$ , or 2.8 and 7.1 times the unfinned value.

#### Analysis of Flow Conditions

The previously developed factors  $E$ ,  $e$ , and  $R$  do not vary greatly with the mass-velocity ratio  $Y$ . Thus, the factors appear to be unique with the internal gas-passage design and have only slight dependence on specific flow conditions. Additional knowledge of the gas- and air-flow properties, however, is of interest because basic gas-heated airfoil designs depend on the absolute values of the internal and external heat-transfer coefficients, which in turn vary considerably with conditions of the flows.

Internal gas flow. - In considering the gas flow, equations (7) and (9) for constant air velocity and gas temperature may be rewritten as

$$h_g = C_3 \frac{(t_s - t_a)_{av}}{(t_{g,m} - t_s)_{av}} = C_4 w^{0.8} \quad (15)$$

or

$$w^{0.8} = C_5 \frac{(t_s - t_a)_{av}}{(t_{g,m} - t_s)_{av}} \quad (16)$$

and

$$\log \frac{(t_s - t_a)_{av}}{(t_{g,m} - t_s)_{av}} = 0.8 \log w - \log C_5 \quad (17)$$

The exponent of  $w$  in equation (9) is the slope of the straight line of equation (17). The data of figure 10 are plotted in figure 11 as the variation of  $(t_s - t_a)_{av} / (t_{g,m} - t_s)_{av}$  with  $w$  on logarithmic coordinates, where the gas-flow exponents appear as the slopes of the lines. The gas-flow exponent is found to be approximately 0.4 rather than 0.8. The exponent 0.8 of equation (9) is the established value for the heating of gases in fully developed turbulent flow in long tubes with no appreciable discontinuity in shape, temperature, or heat transfer. This disagreement illustrates the magnitude of the possible discrepancies between idealized conditions and practical installations.

The installation used in this investigation was occasioned by the cooling of gas in short irregular passages with sizable variations in temperature and heat transfer. These irregularities also exist in full-scale gas-heated airfoils, in addition to other possible effects due to airfoil rotation, foreign particles, and so forth. The longer length or span of most gas-heated airfoils in use allows more fully developed gas flow than is possible in the present installation; however, regions near the entrance to internal flow or any protruding webs, lap joints, fins, stiffeners, bulkheads, partitions, and orifices may all be expected to deviate from the theoretical conditions and equations.

The distance from the point of heat-transfer measurement to the pipe-flow entrance or the nearest upstream shape discontinuity has a very important bearing on the local heat-transfer coefficient. Data presented in reference 9 show that a change in the entrance length or the  $L/D_h$  ratio from 10 to 1 is occasioned by an increase in the heat-transfer coefficient of approximately 2.1 in the laminar pipe-flow regime, where  $h_g \propto w^{1/3}$ . Similar but unpredictable effects are shown in the transition region (Reynolds number  $> 2100$ ). Experiments reported in reference 10 at Reynolds numbers from approximately 26,000 to 56,000 showed that local heat-transfer coefficients vary up to 4.0 times the values at fully developed turbulent flow ( $L/D_h > 15$ ) and that the peak increase in heat transfer occurred between  $L/D_h = 0$  and  $L/D_h = 3$ . These results were obtained with

entrance sections having 45° and 90° bends, sharp-edge openings and sharp edges with short calming sections and upstream orifices. These entrance configurations are similar to those used in the present installation. Similar increases in the gas heat-transfer coefficient at points near the flow entrance are reported in reference 11 in which the coefficient at entrance is from 1.6 to 2.6 times the downstream stabilized value. These results were obtained from heat-transfer investigations of various lengths of electrically heated metal plates placed parallel to an air stream.

From the references cited, it appears that the fully developed turbulent value of  $h_g$  determined from equation (9) should be increased in the order of 2 to 2.5 times to satisfy the gas-flow conditions in the models investigated. Furthermore, the range of Reynolds number investigated with sections A, B, and C lies partly in the transition region and partly in the idealized turbulent region. Thus, the variance of  $h_g$  with  $w^{0.4}$ , as indicated in figure 11, appears feasible because: (a) The exponent of  $w$  is between the 0.33 power for laminar flow and the 0.8 power for turbulent flow; and (b) cooling a boundary layer tends to stabilize the flow and delay transition.

External air flow. - The nature of the external air flow may be determined in a manner similar to that for the gas flow. For constant gas flow, gas temperature, and external air density, equations (7) and (10) to (12) may be combined to give

$$h_a = C_6 \frac{(t_{g,m} - t_s)_{av}}{(t_s - t_a)_{av}} = C_7 v^{(0.5 \text{ or } 0.8)} \quad (18)$$

or

$$\log \frac{(t_{g,m} - t_s)_{av}}{(t_s - t_a)_{av}} = (0.5 \text{ or } 0.8) \log v - \log C_8 \quad (19)$$

Thus, the slope of equation (19) represents the air-velocity exponent. The variation of  $(t_{g,m} - t_s)_{av} / (t_s - t_a)_{av}$  with  $V_0$  is shown on logarithmic coordinates in figure 12 for a gas flow of 325 pounds per hour and a mean gas temperature of 370° F. The velocity exponent for the three sections indicates that the air-flow boundary layer was turbulent over a great extent of the heated surface. The

exact location of the transition from laminar to turbulent flow was not measured and cannot be found because the exact local internal heat-transfer coefficient is unknown. The ratio of turbulent  $h_a$  to laminar  $h_a$  was coincidentally of the same order of magnitude as the indicated increase in the  $h_g$  value caused by pipe-flow entrance irregularities.

#### Heat Transfer in Finned Leading Edge

The chordwise distribution of temperature and heat transfer in the leading-edge region of finned airfoil section C has been determined for the following conditions: gas flow, 325 pounds per hour; tunnel-air velocity, 275 miles per hour; and gas-temperature differential,  $314^{\circ}$  F. The temperature gradient through the tapered fin was found from a series of incremental heat-transmission calculations beginning at the known fin-tip temperature and by utilizing the indicated gas-temperature profile as well as the theoretical gas-film heat-transfer coefficient. The relaxation method presented in reference 12 was used for the fore part of section C to obtain the isotherms shown in figure 13. The external air heat-transfer coefficient determined from the development in figure 13 agreed approximately with the theoretical  $h_a$  (equations (10) and (11)). The heat-flow channels illustrate how the leading-edge fins increase the heat transfer and temperature at the critical stagnation region. Half of the heat flow in the tapered fins is directed into the first 3/8 inch of the airfoil surface.

#### Anti-Icing Evaluation of Airfoil Sections

Airfoil surface-temperature rises in icing conditions may be evaluated from heat-transfer data obtained from dry-air measurements. A general comparative equation is

$$\frac{(h_g A_g)_I (t_{g,m} - t_s)_I}{(h_g A_g)_{II} (t_{g,m} - t_s)_{II}} = \frac{(h_{a,e} A_a)_I (t_s - t_a)_I}{(h_{a,e} A_a)_{II} (t_s - t_a)_{II}} \quad (20)$$

or, for comparing different airfoils with the same internal gas flow and external heated area,

$$(t_s - t_a)_{II} = E(t_s - t_a)_I \frac{(h_{a,e})_I}{(h_{a,e})_{II}} \frac{(t_{g,m} - t_s)_{II}}{(t_{g,m} - t_s)_I} \quad (21)$$

Means of determining surface-temperature rise and heat transfer for a finned airfoil from the known or estimated surface-temperature performance of an unfinned airfoil in either wet- or dry-air flow are given in equation (21). For the specific conditions involved, the factor  $E$  is taken from figure 9 when internal fins and partitions similar to those of sections B and C are used and becomes unity if no change in internal-passage design is involved between conditions I and II. The term  $h_{a,e}$  is the effective external heat-transfer coefficient that is approximated in anti-icing conditions by

$$h_{a,e} \approx h_a X + M c_w \quad (22)$$

where

$$X = 1 + \frac{p_{v,s} - p_{v,a}}{t_s - t_a} \left( \frac{0.622 L_v}{p c_p} \right) \quad (23)$$

and  $L_v$  is the latent heat of vaporization of water (Btu/lb). By assuming straight-line impingement

$$M = \frac{m}{4.45} V_0 \sin \psi \quad (24)$$

In dry-air flow  $h_{a,e} = h_a$  and if conditions I and II are both at the same flight conditions, the term  $(h_{a,e})_I / (h_{a,e})_{II}$  will become unity. If wet air is involved, equation (21) must be solved by a trial-and-error method because of the dependence of  $X$  on  $t_s$ .

By referring to figure 5 and equation (21), a check can be made between the stagnation-point temperature rises of section C for wet air (condition II) and of section A for dry air (condition I) as follows:

$$\begin{aligned} (t_s - t_a)_I &= 38 \approx \frac{1}{E} (t_s - t_a)_{II} \frac{(h_a X + M)_{II} (t_{g,m} - t_s)_I}{h_{a,I} (t_{g,m} - t_s)_{II}} \\ &= \frac{1}{3.78} (28) \frac{[121(4.1) + 118] (370 - 92)}{121 (370 - 89)} = 37.2^\circ \text{ F} \end{aligned}$$

Good agreement is shown between the indicated and calculated temperature rises.

The surface-temperature rise of  $28^{\circ}\text{F}$  above a wet datum air temperature of  $61^{\circ}\text{F}$  (condition II of preceding calculation) may be used to determine the surface-temperature rise above a wet datum air temperature of  $0^{\circ}\text{F}$  for the same flow and heating conditions. Substitution of equation (22) in equation (21) and the trial assumption that  $t_s = 57^{\circ}\text{F}$  gives

$$(t_s - t_a)_{(t_a=0)} = 57 \approx \frac{28 [121(4.1) + 118] (370-57)}{[121(1.78) + 118] (370-89)} = 57.3^{\circ}\text{F}$$

Thus, the resulting stagnation surface-temperature rise above wet air at  $0^{\circ}\text{F}$  is  $57.3/28$  or 2.04 times as much as the rise above  $61^{\circ}\text{F}$  wet air.

The rate of surface heat transfer from the three sections investigated is shown in figure 14 where the product of surface-temperature rise and the external laminar heat-transfer coefficient is plotted in Btu per hour per square foot and in watts per square inch. The local heating rate of the two finned sections is quite high, especially at the leading edge. The surface heat-transfer rates over the leading-edge stagnation regions were approximately as follows:

Airfoil section	Rate of surface heat transfer in stagnation region, (watts/sq in.)
A	10
B	17
C	27

Under these heating intensities and according to previous calculations, finned section C appears able to prevent icing in the most severe icing conditions.

#### REMARKS

By using the factors,  $R$ ,  $E$ , and  $e$ , which are fairly constant over the range of heating and flow conditions investigated, a segment-by-segment design of an internally finned and partitioned airfoil may be made, based on performance data of an unfinned gas-heated airfoil or on an analysis similar to that presented in reference 1. An efficient anti-icing design should then be possible

1281 because of the large improvement at the critical leading-edge region and in the ability of the fins and partitions to extract more of the heat from the gas stream. The number and the size of the fins, as well as the extent of flow partitioning, should be carefully controlled along the gas-stream path in order to balance the drop in gas temperature with the external heat requirements and to provide the optimum chordal and spanwise surface-temperature distribution.

From data of reference 13, calculations were made to indicate that the effect of one fin attached to the leading edge of sections B and C was somewhat more than half as great as in the investigations with two fins per section. The increased heat transfer with increasing number of fins in a given heated gas passage gradually levels off to a maximum beyond which less heat is transferred with additional fins. The fin spacing in this investigation, however, is considerably wider than is required for attaining the point of maximum heat transfer.

For sections B and C, the heat addition due to the internal fins is confined to the leading-edge region of the airfoils, whereas the enlarged partition generally causes increased heat transfer over the entire heated surface. Thus, the sheet-metal fins of section B would probably prove satisfactory for anti-icing designs when combined with reduced gas-flow passage areas that provide a general increase in the level of surface heating.

Several possibilities exist for the matching of local surface heat-transfer rates with local anti-icing heat requirements and are involved in the design selection of

1. Fin number
2. Fin length
3. Fin thickness
4. Fin material
5. Fin location and continuity
6. Gas-flow-passage area
7. Gas-flow-partition location
8. Gas-flow-entrance condition

If localized overheating and underheating of typical gas-heated airfoils (compared to the optimum anti-icing surface temperature of 32° F), such as the hollow propeller blades reported in references 1 to 5, are to be avoided, a careful consideration of all the design items listed should be made and incorporated into the primary airfoil fabrication.

#### SUMMARY OF RESULTS

From an investigation of three gas-heated airfoils, one hollow and two modified with internal fins and partitions for improving anti-icing heat-transfer characteristics, the following results were obtained:

1. The local surface-heating rate for ice prevention on gas-heated airfoils was increased up to 3.5 times by the addition of metal fins attached at the leading edge of the internal gas passage, which was also reduced in area.

2. The surface-heating increase in dry-air flow was from 30 to 80 percent greater at the stagnation point than for the average over the entire heated area of the airfoil sections investigated. The greatest increase in surface heating was obtained with relatively thick tapered fins and with a gas-passage restricting partition.

3. Over the range of air and gas flows investigated, the relative modification effectiveness, defined as the ratio of internal effective conductance between the modified and unmodified airfoil sections, was approximately as follows:

Airfoil section	Relative modification effectiveness	
	Heated-surface average	Stagnation point
Constant thickness fins, center partition	1.6	2.4
Tapered fins, reduced gas-flow passage	2.6	3.7

4. Rates of hot-gas flow through the original unfinned airfoil section were reduced approximately 64 and 86 percent by the addition of constant-thickness or tapered fins, respectively, when the total heat transfer through the heated-surface area was constant.

5. At a gas flow of 325 pounds per hour, a gas-temperature differential of  $310^{\circ}$  F, and an air velocity of 275 miles per hour, the magnitude of surface heat transfer in the stagnation regions was approximately as follows:

Airfoil section	Rate of surface heat transfer in stagnation region, (watts/sq in.)
Unmodified	10
Constant-thickness finned	17
Tapered finned	27

For the tapered-finned section, this heating rate represented a surface-temperature rise in severe icing conditions of approximately  $57^{\circ}$  F above a wet datum-air temperature of  $0^{\circ}$  F.

6. For the flow, heating, and icing conditions presented in the previous paragraph, the temperature drop through a 0.010-inch-thick surface paint coating on the leading edge of the unfinned section was calculated to range from  $10^{\circ}$  to  $15^{\circ}$  F.

7. Fins and partitions in the flow passage of gas-heated airfoils had multiple effects in increasing the local surface heat-transfer rates and in creating design variables that permit more effective control over the chordal and spanwise distribution of heat flow.

Lewis Flight Propulsion Laboratory,  
National Advisory Committee for Aeronautics,  
Cleveland, Ohio, July 7, 1949.

## APPENDIX - SYMBOLS

The following symbols are used in this report:

A	heat-transfer area, sq ft
$A_p$	cross-sectional area of internal flow passage, sq ft
$C_1, C_2, \dots$	constant quantities
c	chord, in.
$c_p$	specific heat of gas at constant pressure, Btu/(lb)(°F)
$c_w$	specific heat of liquid water, 1 Btu/(lb)(°F)
$D_c$	diameter of cylinder, surface of which approximates leading-edge region of given airfoil section, ft
$D_h$	hydraulic diameter, $4A_p/P$ , ft
d	metal thickness measured normal to assumed heat conduction, in.
E	relative modification effectiveness, $\frac{(h_g A_g)_f}{(h_g A_g)_u}$ $\approx \frac{(t_s - t_a)_f (t_{g,m} - t_s)_u}{(t_s - t_a)_u (t_{g,m} - t_s)_f}$ , other conditions being constant
e	modification effectiveness, $\frac{q_{a,f}}{q_{a,u}} \approx \frac{(t_s - t_a)_f}{(t_s - t_a)_u}$ , other conditions being constant
G	gas flow per unit area, $w/3600A_p$ , lb/(sec)(sq ft)
g	acceleration of gravity, ft/sec <sup>2</sup>
h	convective heat-transfer coefficient, Btu/(hr)(sq ft)(°F)
k	thermal conductivity, Btu/(hr)(sq ft)(°F/in.)

L	length of gas travel from entrance of flow system, ft
$L_f$	length of fin from root to tip, in.
M	rate of interception of water, lb/(hr)(sq ft)
m	liquid-water content of ambient air, gm/cu m
P	perimeter of internal-flow passage, ft
p	absolute static pressure, lb/sq ft
$p_v$	pressure of saturated water vapor, lb/sq ft
Q	heat transfer, Btu/hr
$Q_I$	sensible heat content of internal gas flow, Btu/hr
q	rate of heat transfer, Btu/(hr)(sq ft)
$q'$	rate of heat transfer, watts/sq in.
R	gas-flow ratio, $w_f/w_u$ , for which $(t_s - t_a)_{f,av}$ equals $(t_s - t_a)_{u,av}$ corresponding to $w_u$ , other conditions being constant
S	surface distance from stagnation point in chordwise direction, ft
s	surface distance from stagnation point in chordwise direction, in.
T	absolute temperature, °R
t	temperature, °F
V	tunnel-air velocity, mph
v	tunnel-air velocity, ft/sec
w	rate of internal gas flow, lb/hr
X	Hardy's evaporation factor

x	distance from leading edge measured along chord, in.
Y	mass-velocity ratio, $g_0 v_0 / G_u$
y	distance measured normal to chord line, in.
$\rho$	density, $(\text{lb})(\text{sec}^2)/\text{ft}^4$
$\Phi$	center angle of leading-edge cylinder between stagnation point and point on cylinder surface, deg
$\psi$	angle of impingement of water droplet on airfoil surface, deg

## Subscripts:

O	ambient atmospheric conditions
I, II	any specific sets of conditions
a	external air conditions
av	average over heated extent of airfoil section
b	point in airfoil material
e	effective
f	finned airfoil section or fin
g	internal gas conditions
m	mean value in gas stream between inlet and outlet stations
s	external airfoil surface
u	unfinned airfoil section

## REFERENCES

1. Gray, V. H., and Campbell, R. G.: A Method for Estimating Heat Requirements for Ice Prevention on Gas-Heated Hollow Propeller Blades. NACA TN 1494, 1947.

2. Mulholland, Donald R., and Perkins, Porter J.: Investigation of Effectiveness of Air-Heating a Hollow Steel Propeller for Protection against Icing. I - Unpartitioned Blades. NACA TN 1586, 1948.
3. Perkins, Porter J., and Mulholland, Donald R.: Investigation of Effectiveness of Air-Heating a Hollow Steel Propeller for Protection against Icing. II - 50-Percent Partitioned Blades. NACA TN 1587, 1948.
4. Mulholland, Donald R., and Perkins, Porter J.: Investigation of Effectiveness of Air-Heating a Hollow Steel Propeller for Protection against Icing. III - 25-Percent Partitioned Blades. NACA TN 1588, 1948.
5. Darsaw, John F., and Selna, James: A Flight Investigation of the Thermal Performance of an Air-Heated Propeller. NACA TN 1178, 1947.
6. Boelter, L. M. K., Martinelli, R. C., Romie, F. E., and Morrin, E. H.: An Investigation of Aircraft Heaters. XVIII - A Design Manual for Exhaust Gas and Air Heat Exchangers. NACA ARR 5A06, 1945.
7. Martinelli, R. C., Guibert, A. G., Morrin, E. H., and Boelter, L. M. K.: An Investigation of Aircraft Heaters. VIII - A Simplified Method for the Calculation of the Unit Thermal Conductance over Wings. NACA ARR, March 1943.
8. Martinelli, R. C., Weinberg, E. B., Morrin, E. H., and Boelter, L. M. K.: An Investigation of Aircraft Heaters. IV - Measured and Predicted Performance of Longitudinally Finned Tubes. NACA ARR, Oct. 1942.
9. Drexel, Roger E., and McAdams, William H.: Heat-Transfer Coefficients for Air Flowing in Round Tubes, in Rectangular Ducts, and around Finned Cylinders. NACA ARR 4F28, 1945.
10. Boelter, L. M. K., Young, G., and Iversen, H. W.: An Investigation of Aircraft Heaters. XXVII - Distribution of Heat-Transfer Rate in the Entrance Section of a Circular Tube. NACA TN 1451, 1948.

11. Joyner, Upshur T.: Experimental Investigation of Entrance-Region Heat-Transfer Coefficients. NACA ARR 3K01, 1943.
12. Emmons, Howard W.: The Numerical Solution of Partial Differential Equations. Quart. Appl. Math., vol. II, no. 3, Oct. 1944, pp. 173-195.
13. Biermann, Arnold E.: Heat Transfer from Cylinders Having Closely Spaced Fins. NACA TN 602, 1937.

TABLE I - DIMENSIONS OF NACA 0012 AIRFOIL SECTIONS

[Angle of attack, 0 deg; chord 10 in.]



Dimension	Section A	Section B	Section C
Skin thickness (except leading edge), in.	0.12	0.12	0.12
Skin thickness (leading edge), in.	.62	.62	.62
Leading-edge cylinder diameter, in.	.40	.40	.40
Span of section, in.	1.87	1.87	1.87
Gas-passage area, sq. in.	3.14	2.82	1.70
Passage perimeter, in.	8.82	18.82	16.34
Insulated length of perimeter, in.	.82	.82	1.94
Length of fins, in.		2.50	2.25
Thickness of fins, in.		.06	.02 to .25
Maximum chordal thickness of insulated partition, in.	1	1	2.25



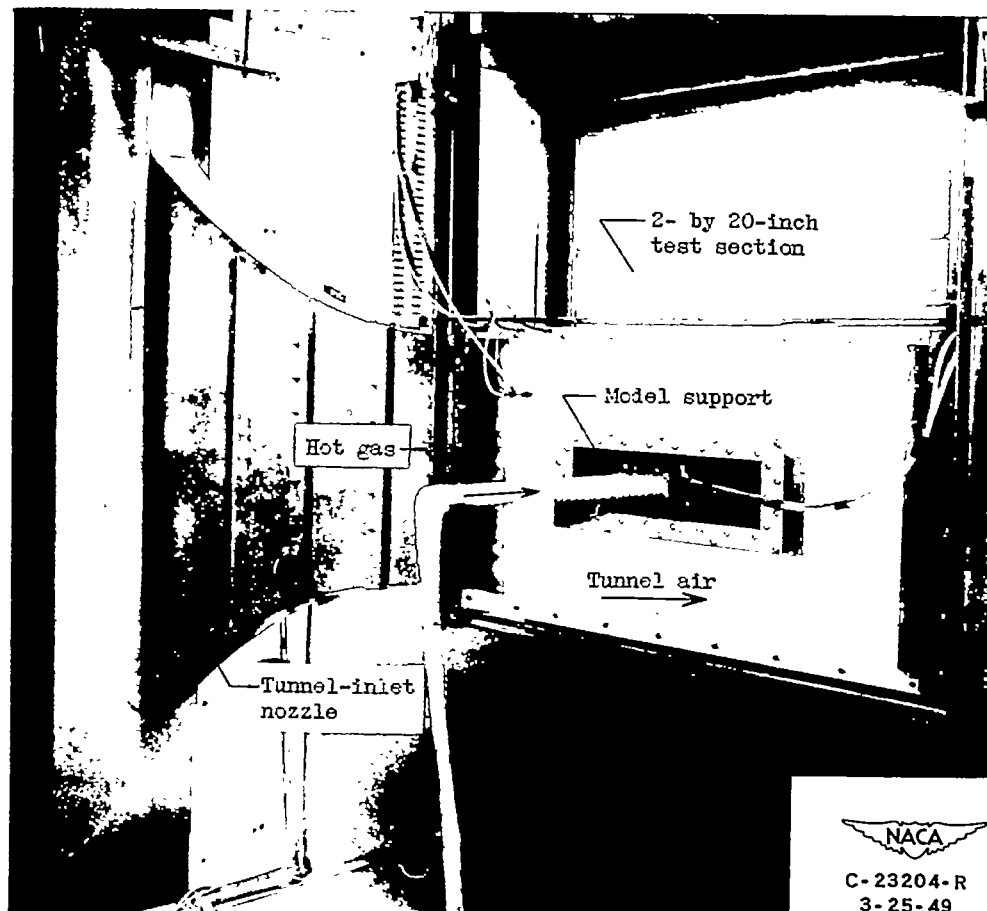


Figure 1. - Installation of gas-heated airfoil section in 2- by 20-inch duct tunnel.



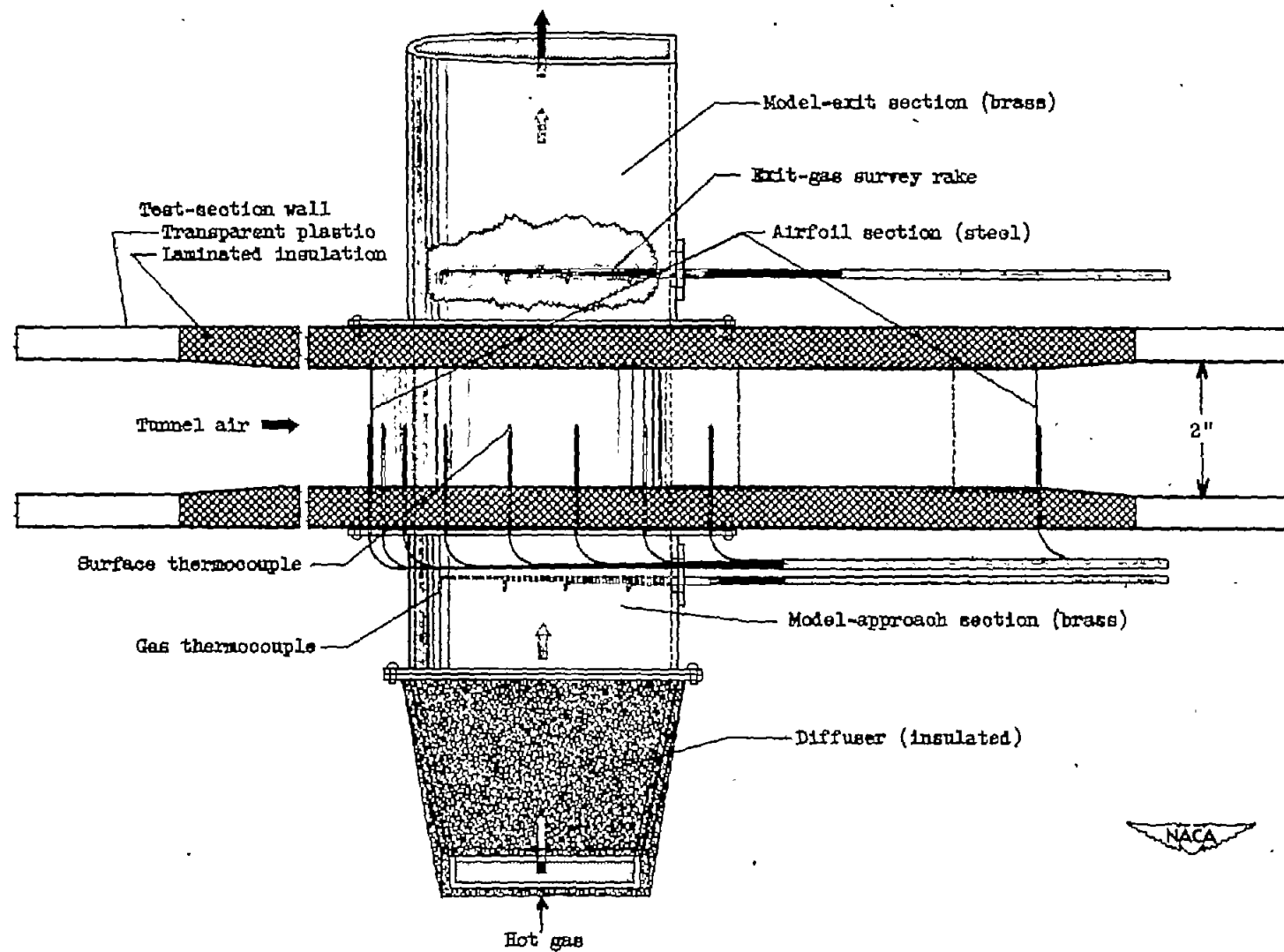
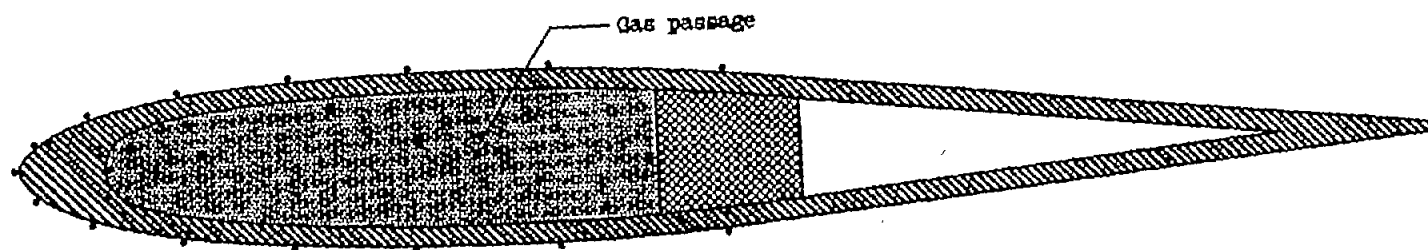
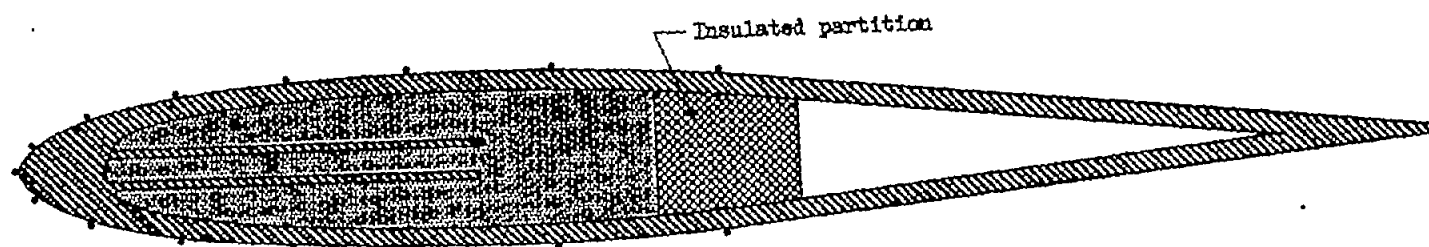


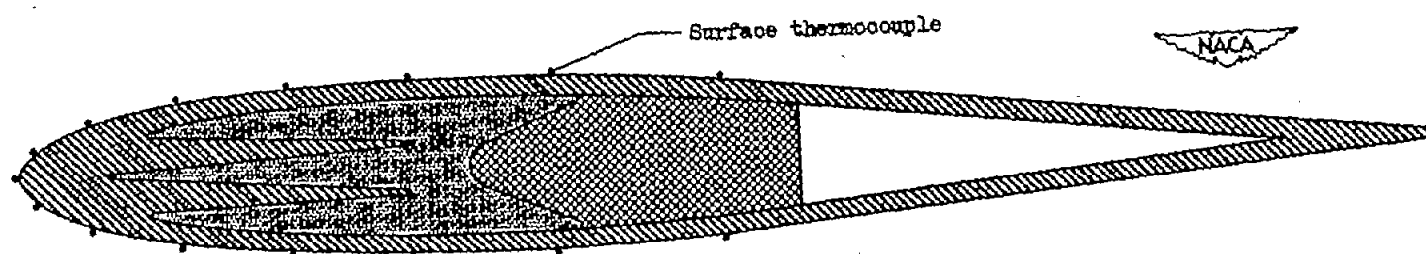
Figure 2. - Top view of unfinned gas-heated airfoil section mounted in 2- by 20-inch duct tunnel.



(a) Section A (unfirmed, center partition).



(b) Section B (constant thickness fins, center partition).



(c) Section C (tapered fins, reduced gas passage with enlarged partition).

Figure 3. - Details of three gas-heated steel airfoil sections.

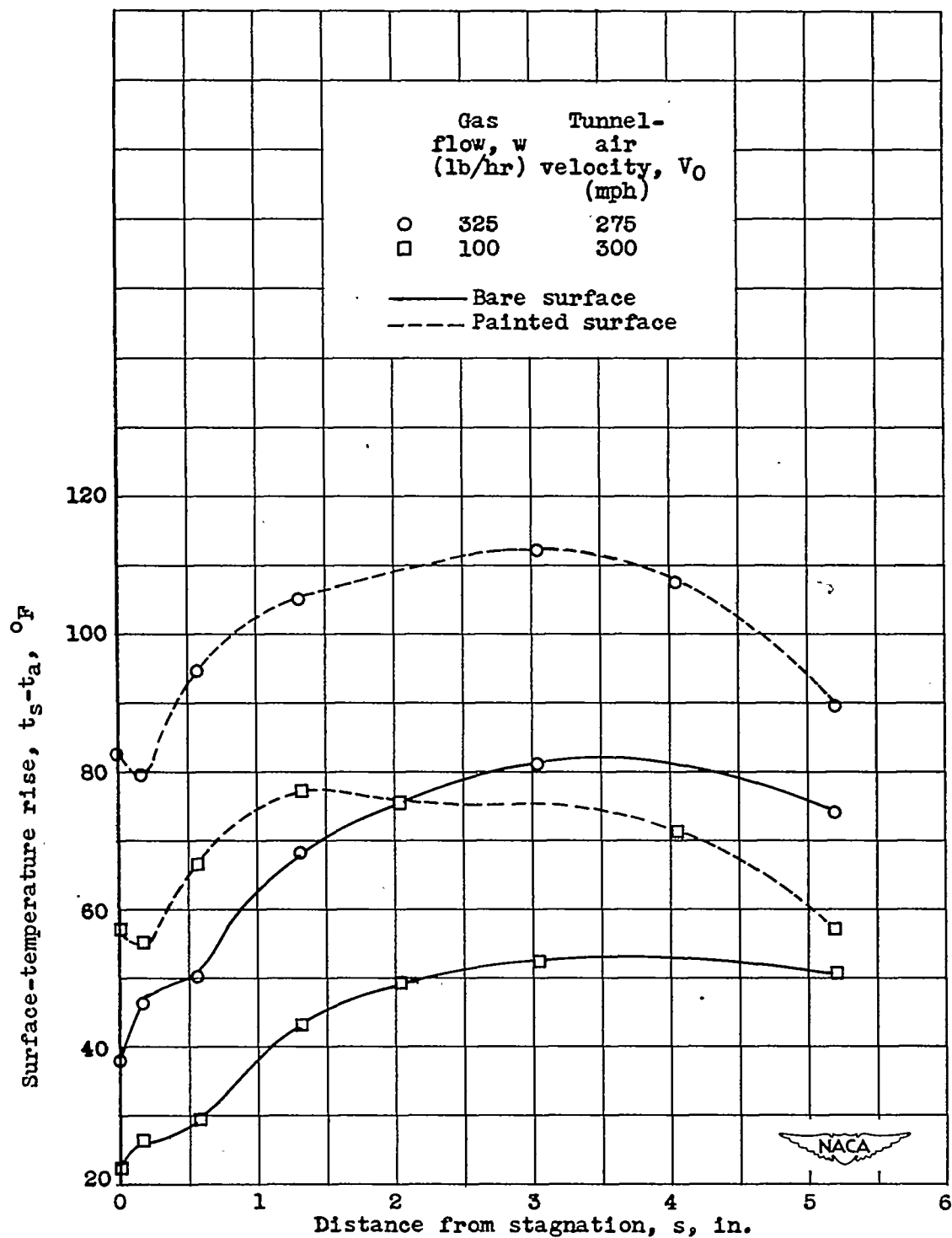


Figure 4. - Chordwise distribution of surface-temperature rise for bare and painted airfoil section A under two flow conditions. Mean gas temperature, 370° F.

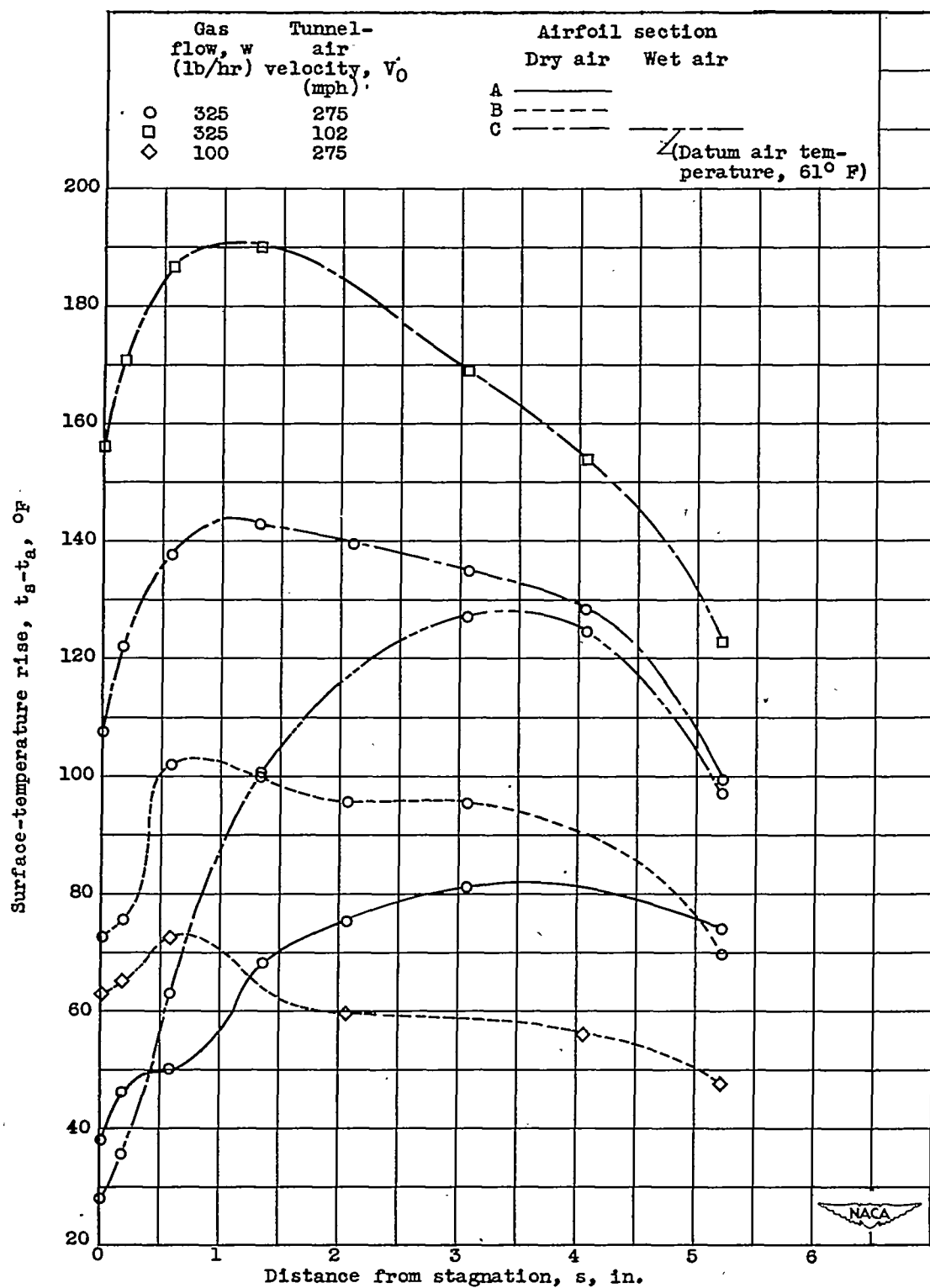


Figure 5. - Typical chordwise distributions of surface-temperature rise for three airfoil sections at various flow conditions. Mean gas temperature, 370° F.

1281

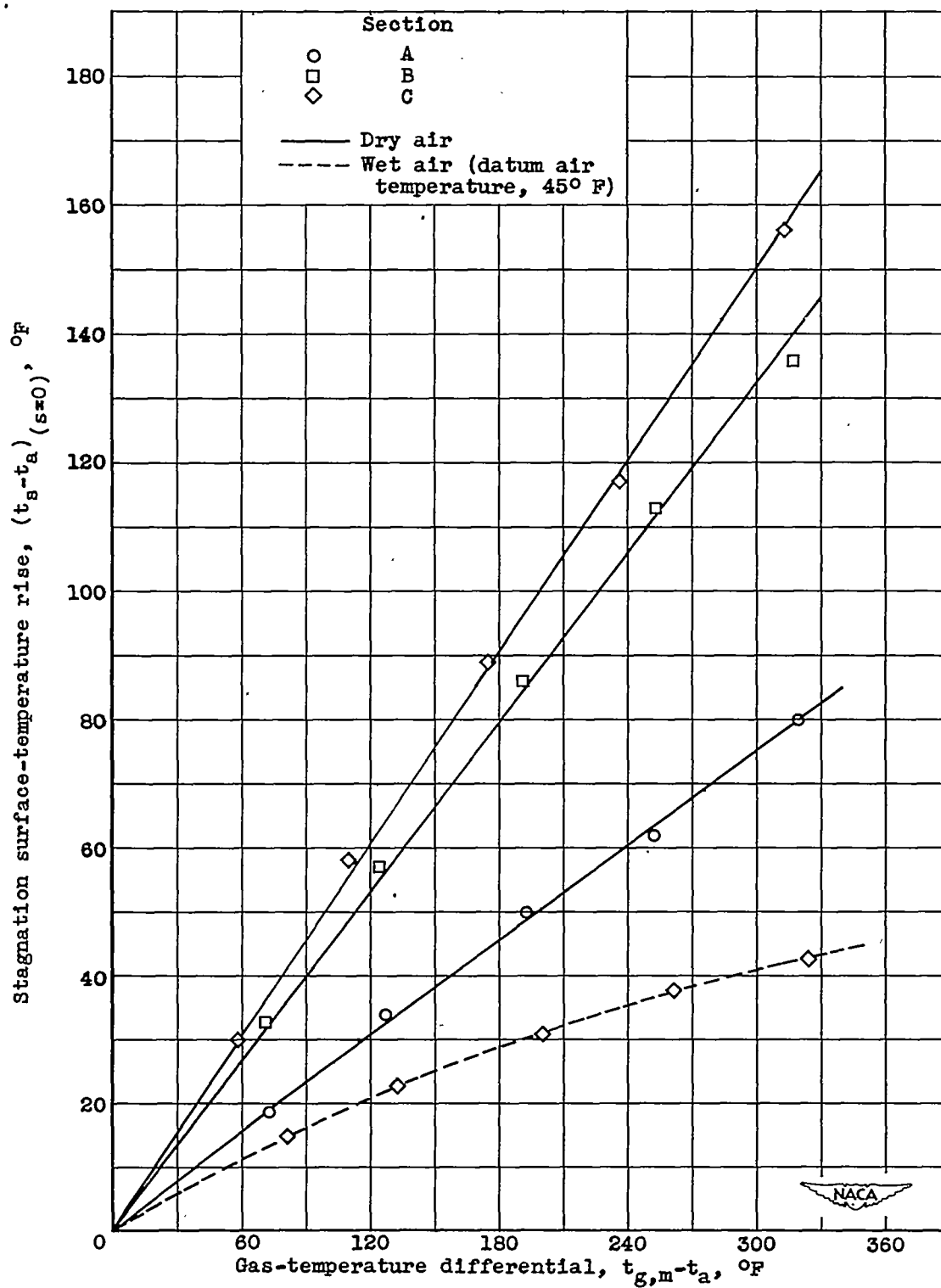


Figure 6. - Effect of gas temperature on surface-temperature rise at stagnation point. Gas flow, 325 pounds per hour; tunnel-air velocity, 102 miles per hour.

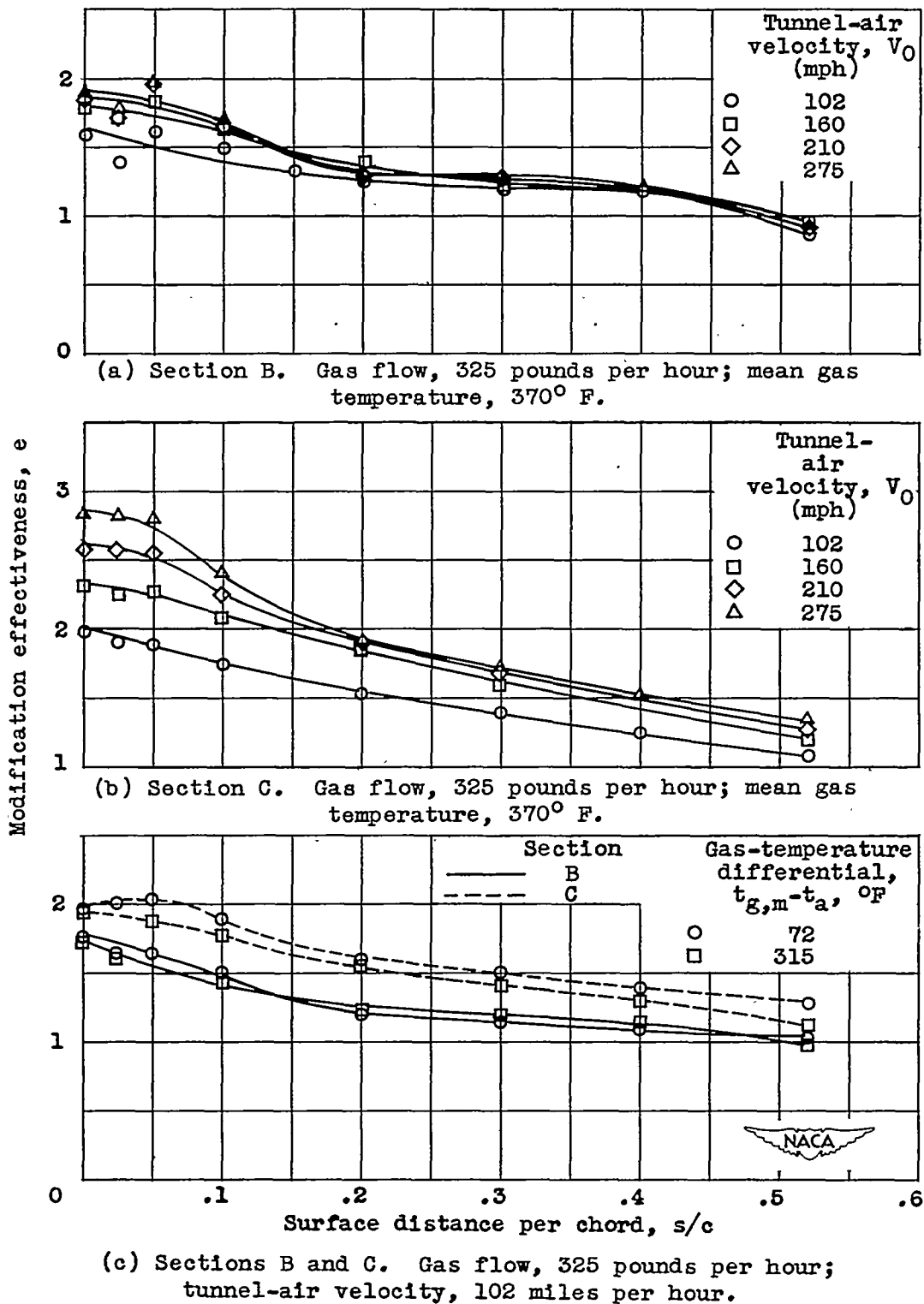
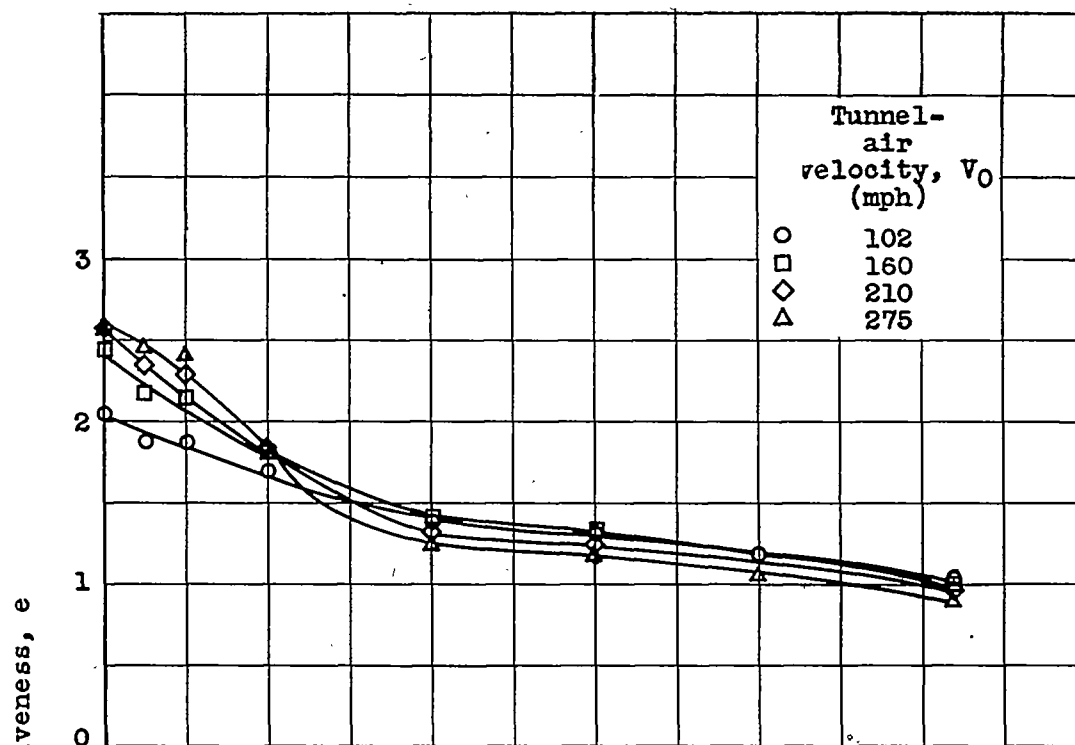
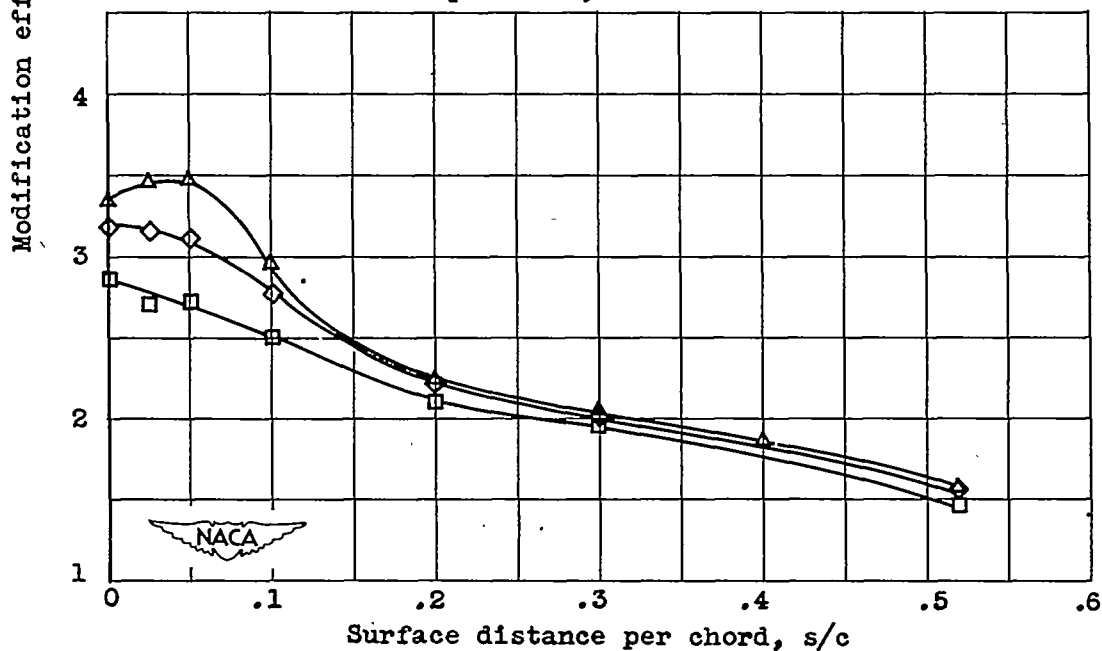


Figure 7. - Chordwise variations of modification effectiveness for sections B and C.

1281



(d) Section B. Gas flow, 100 pounds per hour; mean gas temperature,  $370^\circ\text{F}$ .



(e) Section C. Gas flow, 100 pounds per hour; mean gas temperature,  $370^\circ\text{F}$ .

Figure 7. - Continued. Chordwise variations of modification effectiveness for sections B and C.

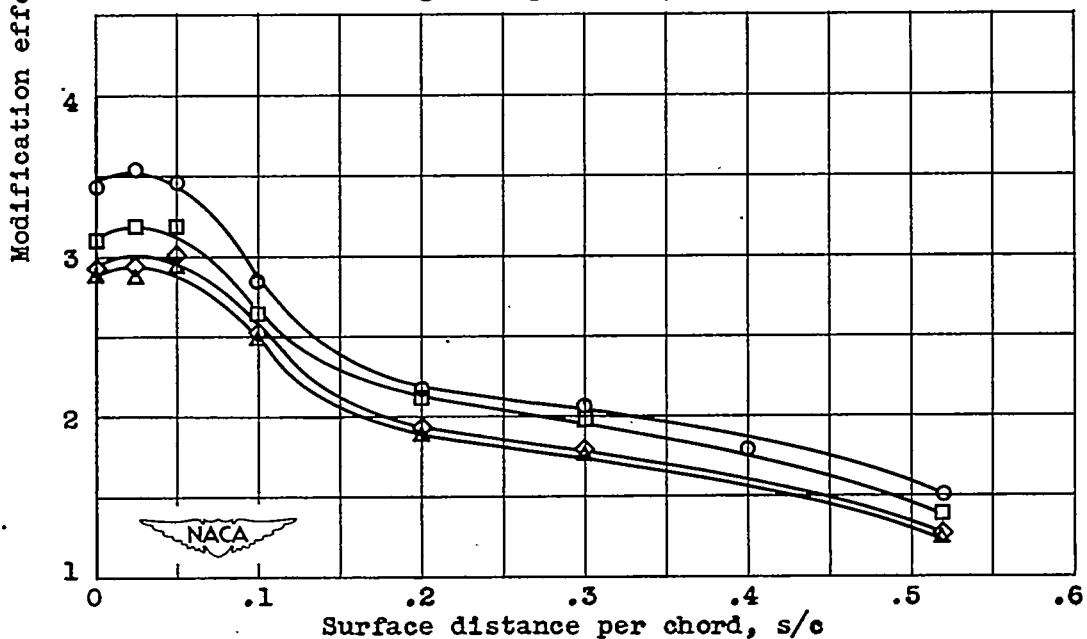
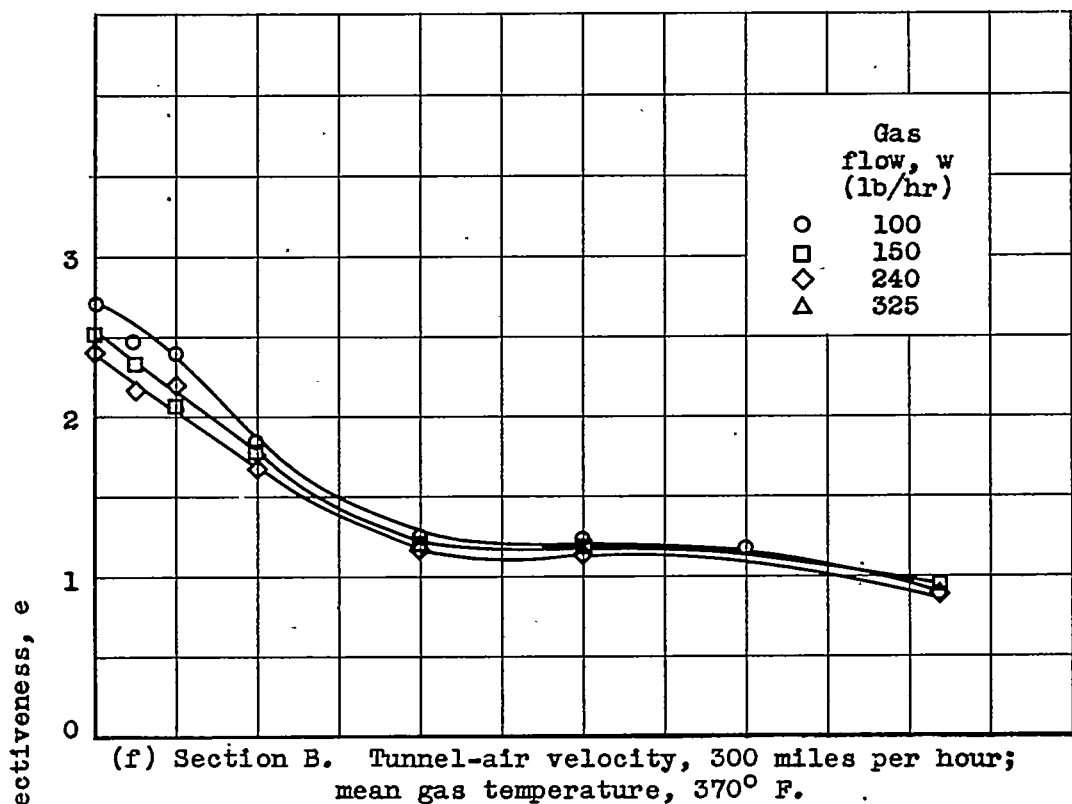


Figure 7. - Concluded. Chordwise variations of modification effectiveness for sections B and C.

1281

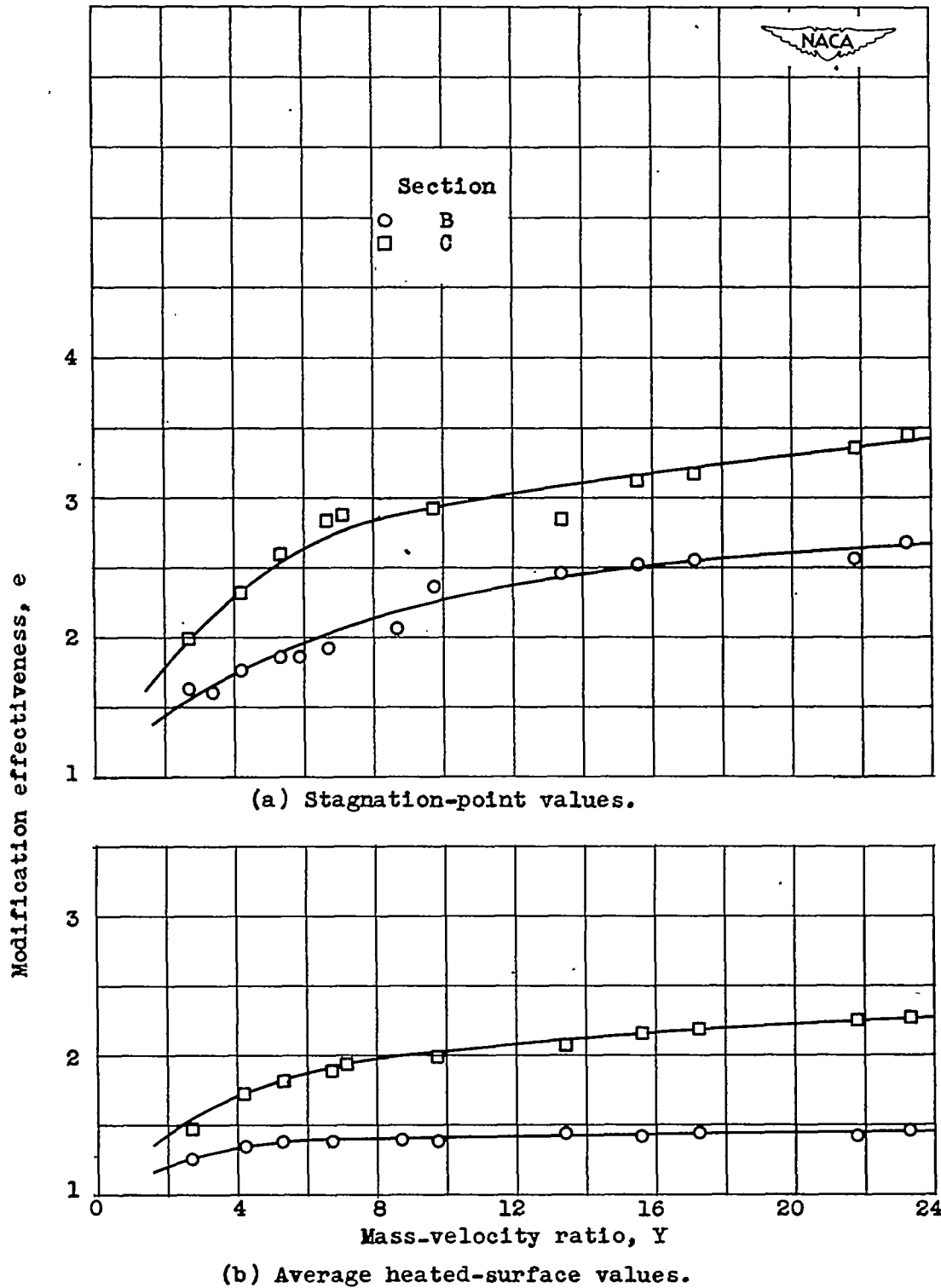


Figure 8. - Modification effectiveness as function of mass-velocity ratio. Mean gas temperature, 370 °F.

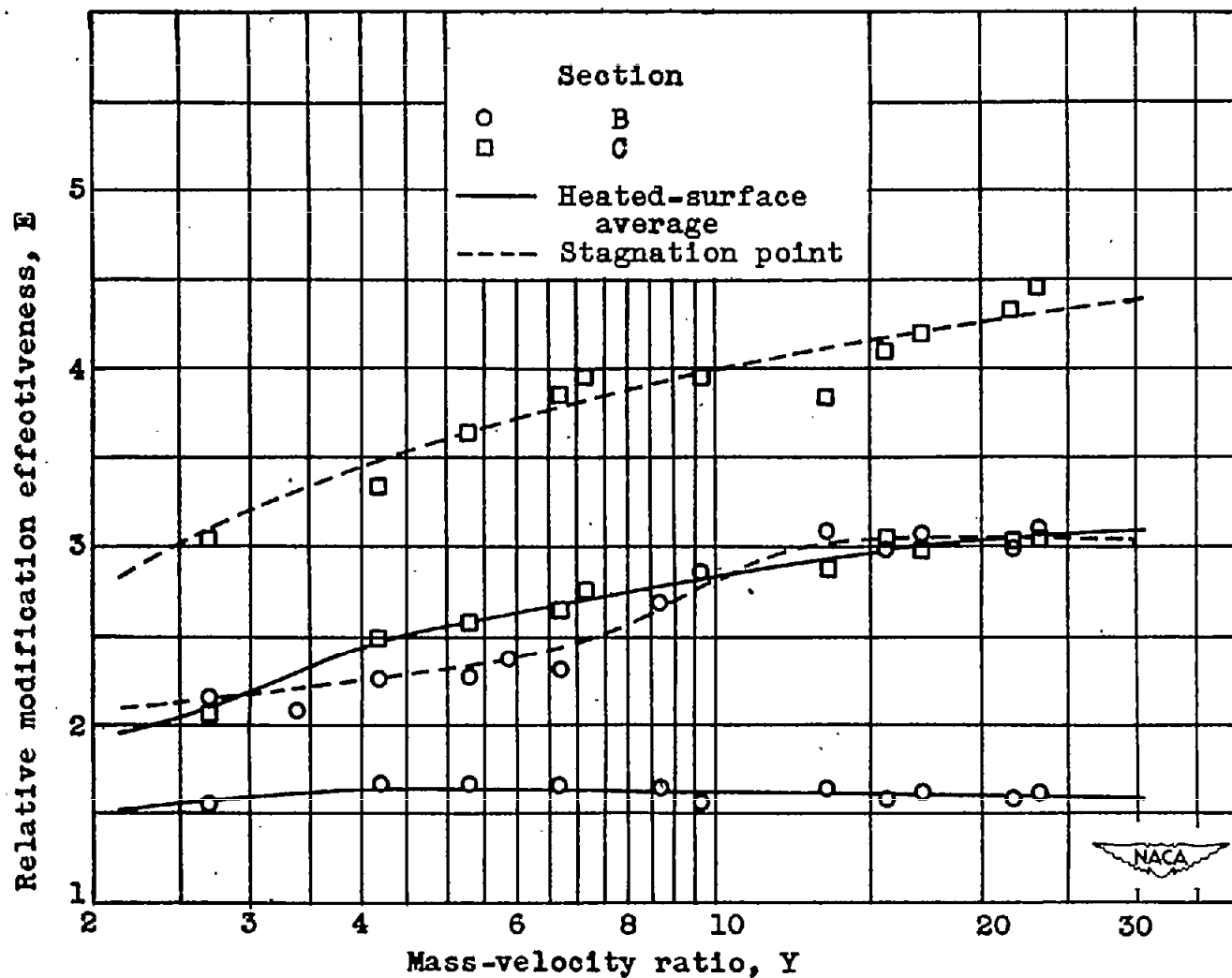


Figure 9. - Relative modification effectiveness as function of mass-velocity ratio. Mean gas temperature, 370° F.

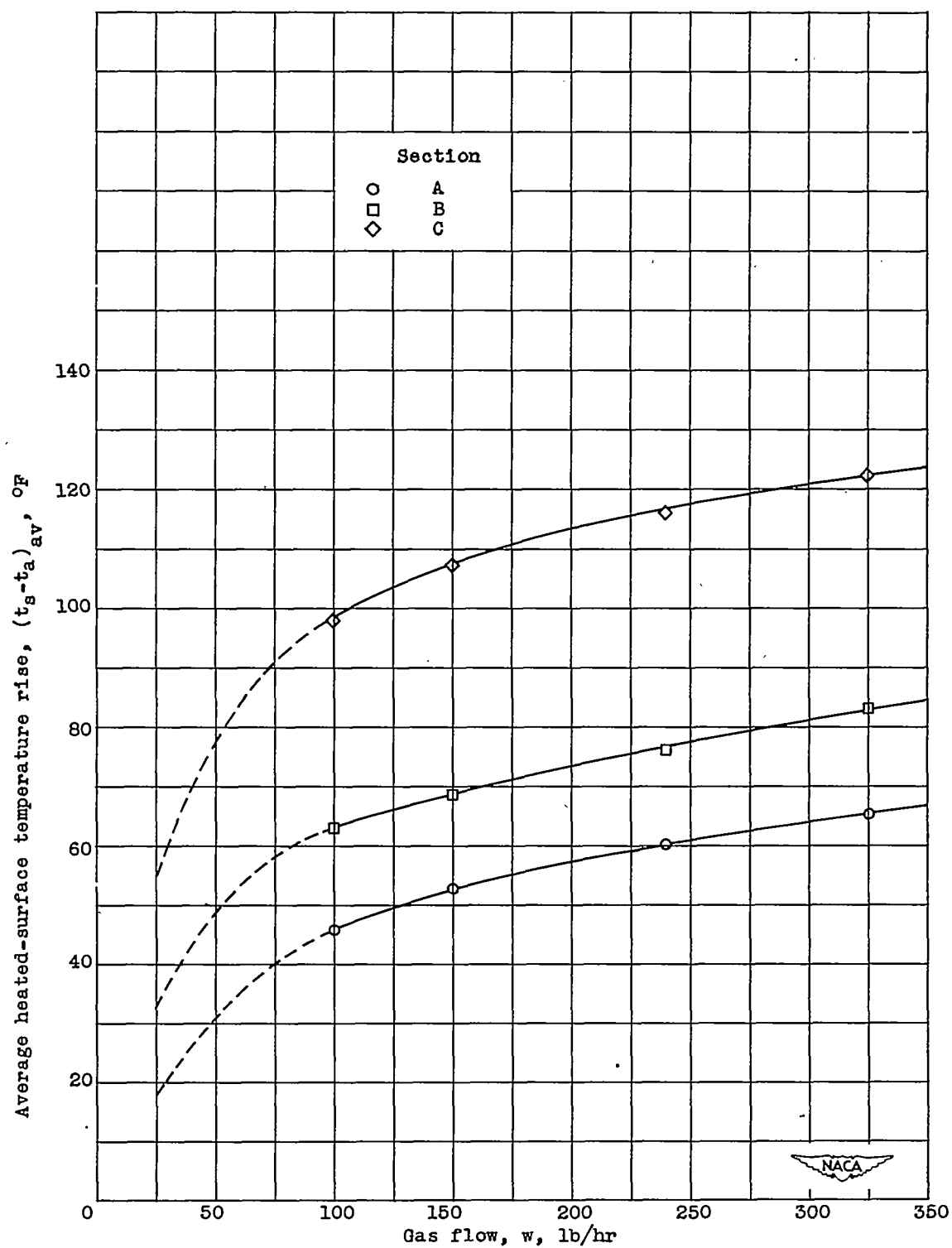


Figure 10. - Average heated-surface temperature rise as function of gas flow. Tunnel-air velocity, 300 miles per hour; mean gas temperature, 370° F.

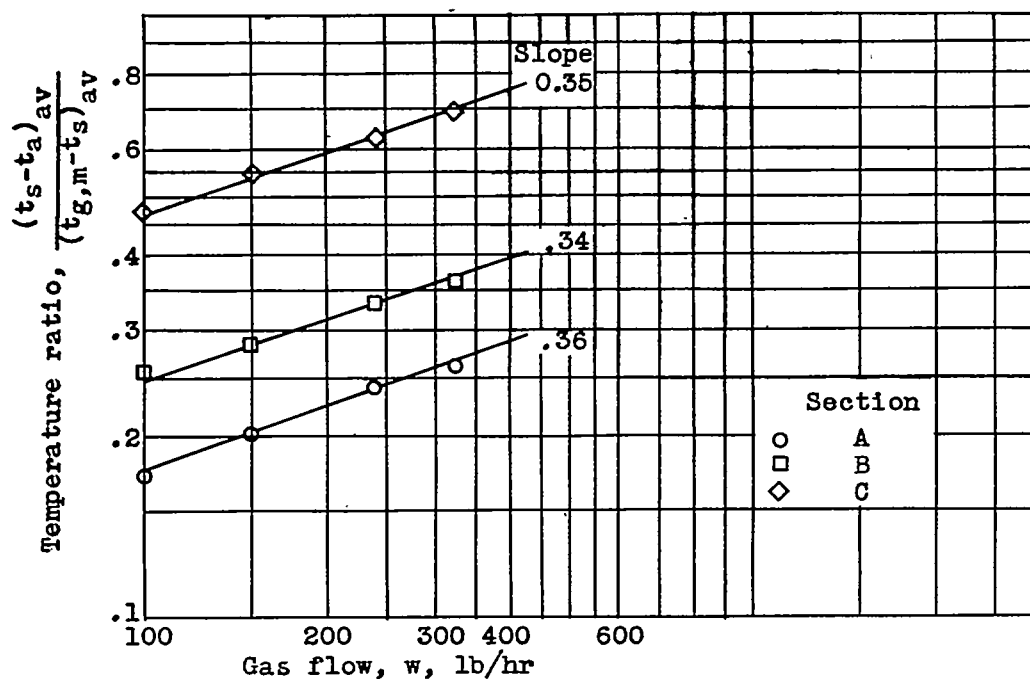


Figure 11. - Temperature ratio as function of gas flow. Tunnel-air velocity, 300 miles per hour; mean gas temperature, 370° F.

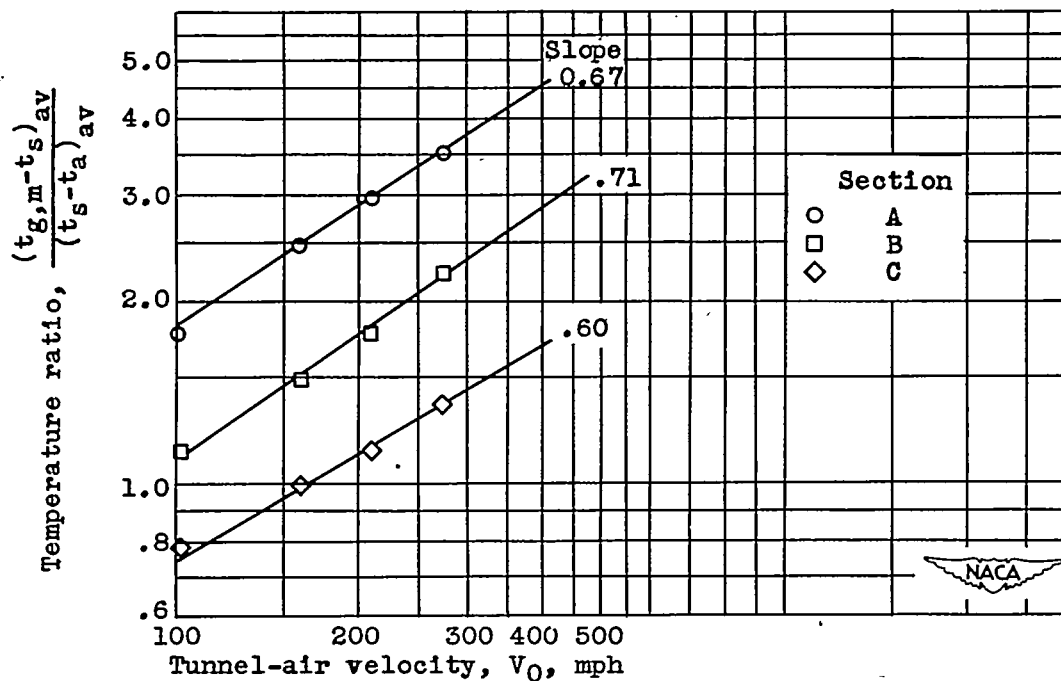


Figure 12. - Temperature ratio as function of tunnel-air velocity. Gas flow, 325 pounds per hour; mean gas temperature, 370° F.

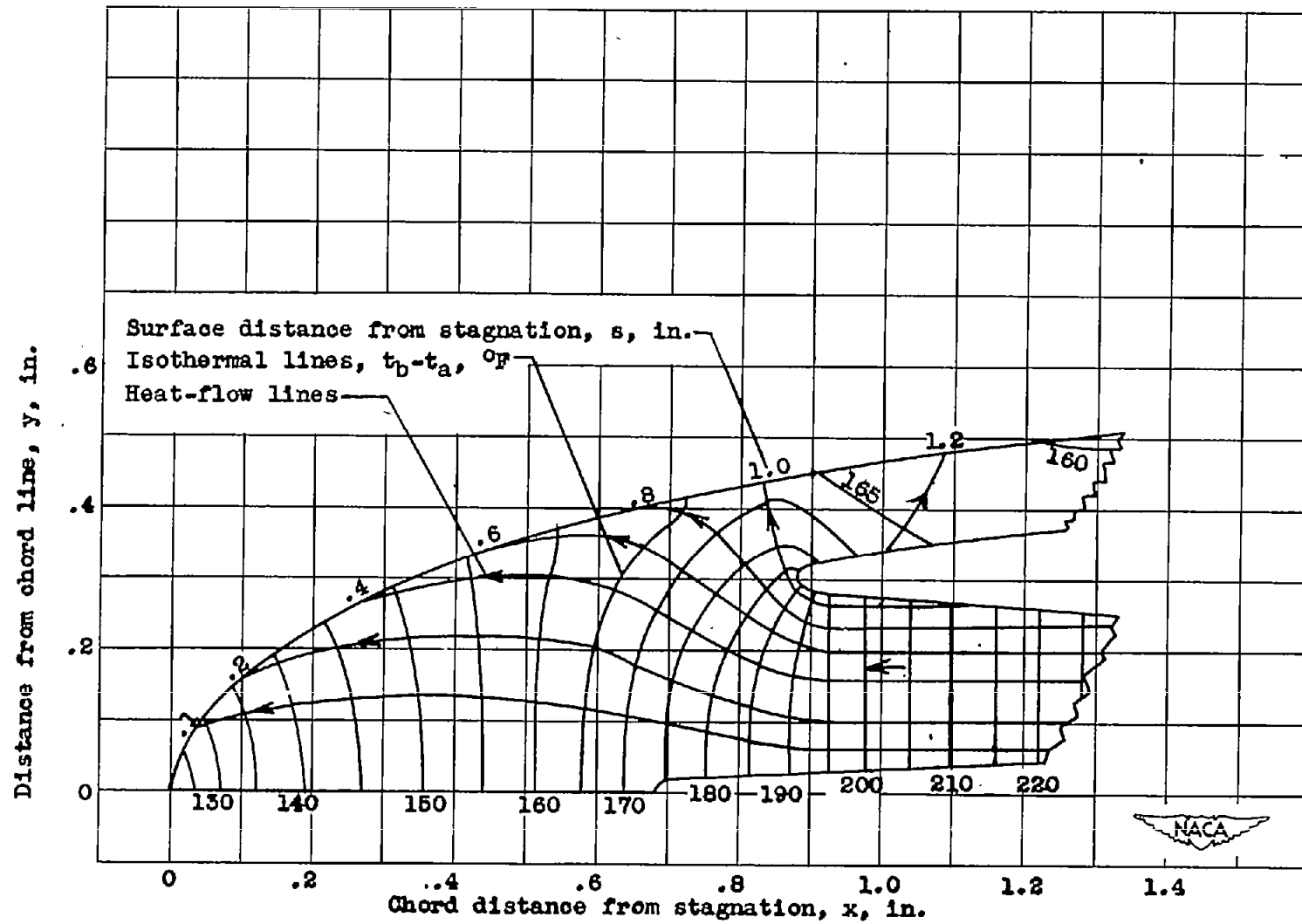


Figure 13. - Temperature pattern along center cross section of section C. Gas flow, 325 pounds per hour; tunnel-air velocity, 275 miles per hour; gas-temperature differential,  $314^{\circ}\text{F}$ .

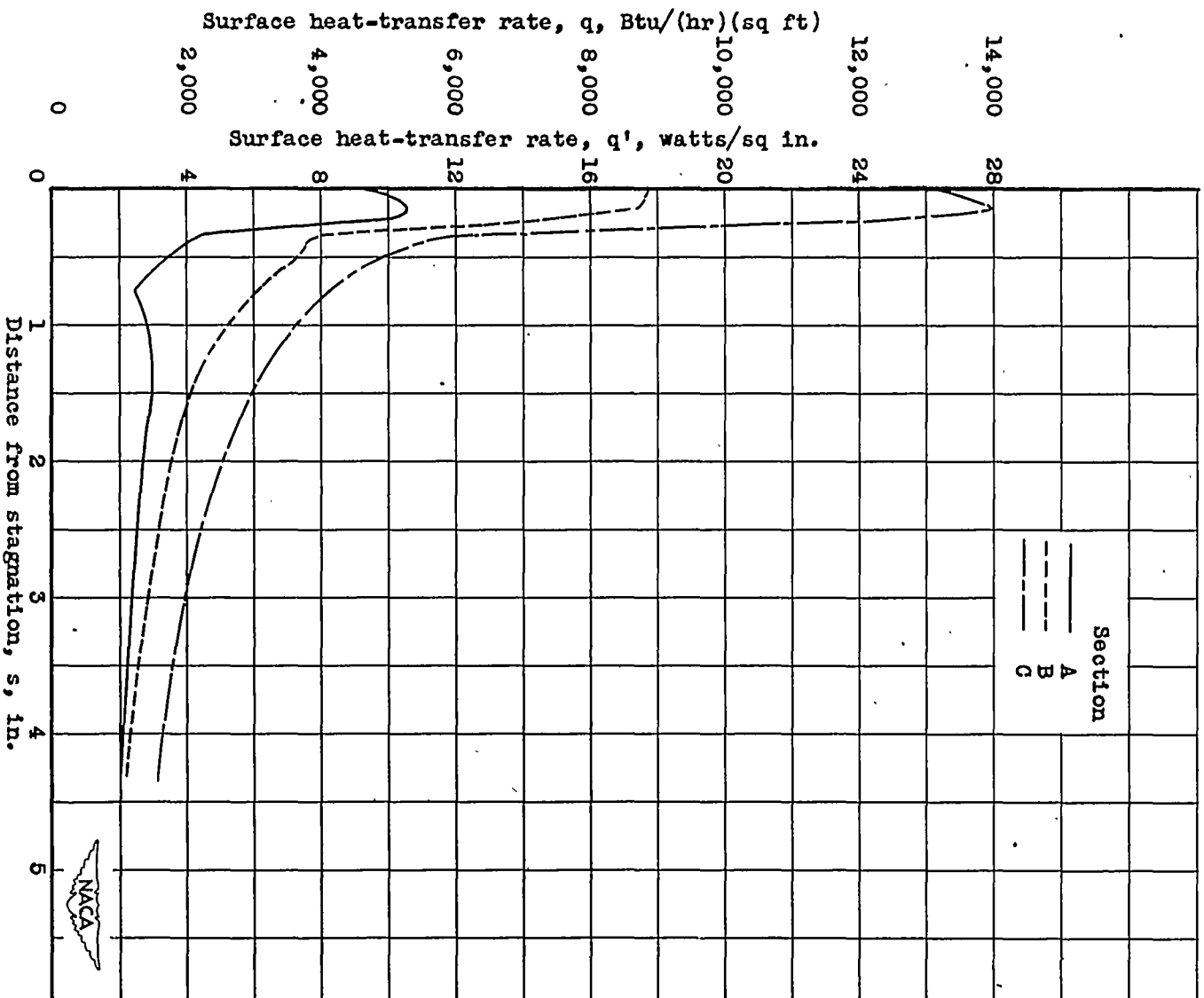


Figure 14. - Chordwise variation of surface heat-transfer rates. Gas flow, 325 pounds per hour; tunnel-air velocity, 275 miles per hour; gas-temperature differential, 310 °F.